Influence of nitrogen ion implantation on deformation and fatigue properties of TiNi shape memory alloy wire

K. TAKEDA[1], K. MITSUI[2], H. TOBUSHI[1],
N. LEVINTANT-ZAYONTS[3], S. KUCHARSKI[3]

[1] *Department of Mechanical Engineering*
Aichi Institute of Technology
1247 Yachigusa, Yakusa-cho, Toyota
Aichi 470-0392, Japan
e-mails: tobushi@aitech.ac.jp, q11801qq@aitech.ac.jp

[2] *Masupuro Denkoh Corp.*
80 Jounou, Asada-cho, Nisshin
Aichi, 470-0194, Japan
e-mail: p10726pp@gmail.com

[3] *Institute of Fundamental Technological Research*
Polish Academy of Sciences
Pawinskiego 5B
02-106 Warsaw, Poland
e-mails: neonila@ippt.pan.pl, skuchar@ippt.pan.pl

A SHAPE MEMORY ALLOY (SMA) is expected to be applied as intelligent material since it shows the unique characteristics of the shape memory effect and superelasticity. Most SMA elements, with these characteristics, perform cyclic motions. In these cases, fatigue of SMA is one of the important properties in view of evaluating functional characteristics. The fatigue properties are complex since they depend on stress, strain, temperature and time. If SMA is implanted by high energy ions, the thermomechanical properties may change, resulting in long fatigue life. In the present study, the nitrogen ion implantation was applied to modify TiNi SMA wire surface and the influence of implantation treatment on the tensile deformation and bending fatigue properties was investigated.

Key words: shape memory effect, titanium-nickel alloy, nitrogen ion implantation, superelasticity, fatigue.

1. Introduction

PUBLICATIONS FROM PREVIOUS YEARS confirm that the TiNi-matrix alloys are among the best shape memory alloys (SMA). In the growing number of TiNi SMA applications, these materials should fulfill high requirements of corrosion,

wear and fatigue resistance. On the other hand, the application of SMA has some limitations, particularly in thermo-cyclic loading cases, when structural components can be damaged due to fatigue [1]. In these cases, fatigue of SMA is one of the important properties in view of evaluating functional characteristics as SMA elements.

It is known that the problem of creating a protective surface coating for the SMA is the most important for its applications such as medical implants, orthopedic devices, surgical tools, endodontic instruments and orthodontic wires in dentistry [2, 3]. In general, ion implantation is a surface engineering process where ions of different materials are accelerated in electrical field and penetrate into a near-surface region of a solid. Generally, the ion-implantation process is used to change the physical, chemical or electrical properties of the solids [4]. In the process, a large number of ions bombard a surface, penetrate in near-surface region interacting with the substrate atoms and a thin surface layer is generated having different properties than the bulk material. In surface engineering, the above process is applied to improve mechanical properties such as hardness, wear and fatigue resistance [5]–[8].

The ion implantation process is performed in a vacuum chamber at very low pressure (10^{-4} to 10^{-5} Torr). The main parameters of this process are the ion dose, i.e., the number of ions per unit area (typically, 10^{15} to 10^{18} J/cm^2) and the ion beam energy. The typical range of energy used in surface engineering is 50 keV to 200 keV. Characteristic depth of the ion penetration is a fraction of a micron (about several hundred nanometers). The thin layers generated in the ion-implantation process are investigated using fundamental methods such as: XRD (X-ray diffraction) – for phase composition; GIXRD (grazing incidence X-ray diffraction) – for microstructure and phase composition; AES (Auger electron spectroscopy) – for composition as a function of depth; TEM (transmission electron microscopy) – for microstructure; RBS (Rutherford backscattering spectrometry) – for depth profile of elements.

There are few papers concerning the effect of ion implantation on characteristic temperatures, structure changes and mechanical properties of TiNi shape memory alloy. In [5] the effect of Al ion implantation (with high doses D1 = 1×10^{21} J/cm^2 at 50 keV and D2 = 3×10^{21} J/cm^2 at 150 keV) on shape memory properties of TiNi has been presented. The results of RBS measurement show that the modified layer has a thickness of 400 nm and in the region 100 nm from the surface high titanium concentration has been observed. The XRD analysis of phase composition revealed that the modified layers were complex composites of implanted ions and secondary phases of TiNi. Aluminum ion implantation changed the "shape memory behavior" of TiNi: the transformation temperature decreased and martensite phase accommodation after R-phase deformation proceeded at low stress when compared to non-implanted samples.

Paper [6] shows investigation of mechanical properties such as hardness and elastic modulus of boron and nitrogen ion implanted TiNi orthodontic wires of 1.5 mm diameter (doses of 1×10^{16}, 5×10^{16} and 1×10^{17} J/cm^2, and energy of 150 keV). Hardness H and elastic modulus E were specified using indentation test with ultra-low (0.5 $\sim$ 20 mN) load. For large 1×10^{17} J/cm^2 boron dose, a significant increases in hardness and elastic modulus were observed (respectively 7.70 GPa and 110 GPa for implanted and 4.2 GPa and 65 GPa for non-implanted). GIXRD measurement shows that ion implantation causes formation of amorphous layer about 250–300 nm.

In [9] it has been shown that after nitrogen ion implantation (doses of 2×10^{17} J/cm^2 and 2×10^{18} J/cm^2) the thickness of modified layer is around 300 nm and the following effects are observed: reduction of Ni content in the 30–40 nm layer near the surface (AES method), increase in hardness and improvement of sliding wear resistance. The reduction of Ni content improves the biocompatibility of TiNi alloy; furthermore, the increase in hardness is extended to the regions much deeper than the ion penetration depth. Analysis of phase and structure composition (XRD, HTEM) in [10] reveals that the nitrogen implanted layer (1×10^{18} J/cm^2) is not homogeneous; one observes existence of the well-defined three layers having a different phase and chemical composition. From the surface to a depth of 80 nm the sample has an amorphized structure in the form of two sub-layers: the first is a Ti- and N-rich nano-crystalline and/or amorphous-like and the second – Ni-rich crystalline. In the depth ranging between 80 and 160 nm the material has a defected Ti-rich crystalline microstructure. Below the 160 nm, an unaffected grain structure of the parent material is seen. Several recent studies concerning dental instruments have reported that the ion implantation can improve the cyclic fatigue resistance of rotary nickel-titanium instruments [11], [12]. In [11] it has been shown that nitrogen ion-implanted (2.5×10^{17} J/cm^2) TiNi endodontic instruments reached a significantly higher cycle number before fracture (510 cycles) when compared with non-implanted instruments (381 cycles). Such studies suggest that an industrial implementation of the ion implantation process would produce rotary nickel-titanium instruments with a longer working life.

In this paper, we report and discuss the influence of nitrogen ion implantation on the phase transformation temperature, tensile deformation and bending fatigue properties of TiNi SMA wires.

2. Experimental method

2.1. Materials and specimen

The materials used in the experiment were Ti-50.85 at.% Ni SMA wires with a diameter of 0.5 mm. They were polycrystalline and produced by Furukawa

Techno Material Co., Ltd. The material shows superelasticity at room temperature. The DSC curve and stress-strain curve will be shown in Figs. 2 and 3, respectively. Nitrogen ion was implanted in the material. The detail of nitrogen ion implantation will be explained in the next section. The length of the specimen was 80 mm.

2.2. Nitrogen ion implantation

The surface of the wire-samples was cleaned using alcohol and hot acetylene. TiNi wire-samples were gripped in special holders (Fig. 1) that enabled the ion beam treatment of two opposite sides. The TiNi SMA wire was ion-implanted from two opposite directions by nitrogen ion beam (see directions and centers of ion-implantation C_i in Fig. 5). Nitrogen ion implantation was carried out using semi-industrial implanter IMJON (Institute of Fundamental Technological Research, Polish Academy of Sciences, Warsaw). The energy of nitrogen ion beam was 50 keV and two doses of nitrogen ions were applied: 5×10^{16} J/cm^2 and 1×10^{18} J/cm^2. The surface color of the ion-implanted wire with 1×10^{18} J/cm^2 is deeper gold than that with 5×10^{16} J/cm^2.

Fig. 1. View of ion implanted TiNi wire-samples in special holder.

2.3. Experimental procedure

In order to investigate the influence of nitrogen ion implantation on the phase transformation temperature, tensile deformation and bending fatigue properties, the following three kinds of test were carried out:

(1) DSC test

The phase transformation temperature was measured by the differential scanning calorimetry (DSC) test. In the test, DSC-60 produced by Shimadzu Co., Ltd was used. The heating and cooling rate was 4 K/min.

(2) Tension test

In the tension tests, EZ-Graph produced by Shimadzu Co., Ltd was used. An extensometer with a gauge length of 50 mm was used to measure displacement. The tension tests were carried out under a constant strain rate $d\varepsilon/dt = 1.67 \times 10^{-4}$ s^{-1} in air at room temperature.

(3) Bending fatigue test

In the fatigue test, an alternating-plane bending fatigue test machine [13] was used. The test for alternating-plane bending fatigue was carried out in air at room temperature. The maximum bending strain appeared on the surface of the wire at the point of center of ion implantation (see points C_i in Fig. 5). The frequency f was found to be 3.33 Hz (200 cpm). A motion analysis microscope VW-6000 produced by Keyence Co., Ltd was used to observe the fracture surface of the specimen.

3. Transformation temperature

The DSC thermograms for three kinds of wires: with non-implanted surface, ion-implanted with 5×10^{16} J/cm^2 and with 1×10^{18} J/cm^2, are shown in Fig. 2. In the cooling process, two peaks due to the rhombohedral phase (R-phase) transformation (RPT) and the martensitic transformation (MT) are observed clearly in the case of the ion-implanted wires. However, the two peaks are not clearly visible in the case of the non-implanted wire. If the dose of ion implantation increases, the RPT start and finish temperatures R_s and R_f and the MT finish temperature M_f increase. However, the MT start temperature M_s is almost constant. In the heating process, two peaks due to both reverse transformations of M-phase to R-phase and R-phase to A-phase are observed in the case of the non-implanted wire. However, one peak appears in the case of the ion-implanted wires. If a dose of ion implantation increases, the M-phase to R-phase reverse transformation start temperature R'_s and R-phase to A-phase reverse transformation finish temperature A_f increase.

The transformation temperature width A_f–R'_s of the two reverse transformations becomes narrow. Although the ion-implanted region is limited in the surface layer, temperature of the wire increases during the ion implantation process. If the shape memory processing temperature is high, the phase transformation temperature increases. Therefore, the same as in the shape memory processing, the phase transformation temperature increases due to the temperature rise during the ion implantation process. The non-implanted wire is the austenite phase at room temperature. The ion-implanted wire with 1×10^{18} J/cm^2 is the R-phase at room temperature.
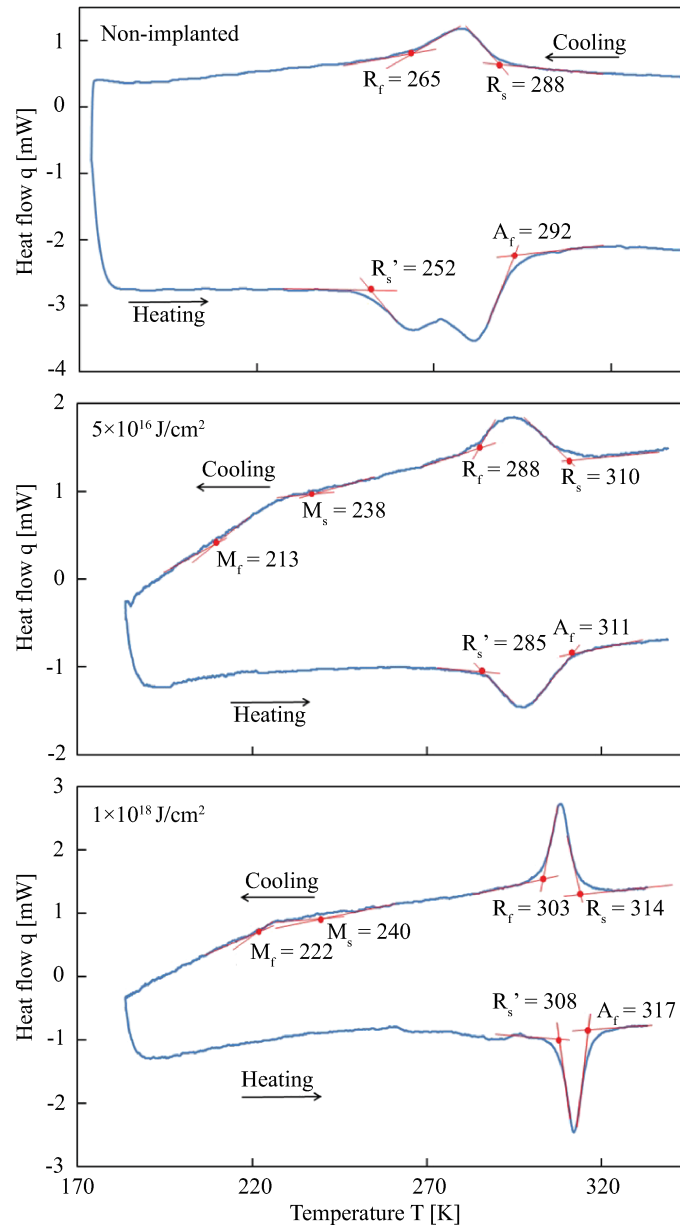
Fig. 2. DSC curves of ion-implanted and non-implanted SMA wires.

4. Tensile deformation property

The stress-strain curves of three kinds of wires obtained by the tension test at room temperature are shown in Fig. 3. In Fig. 3, S_M, F_M, S_A and F_A denote
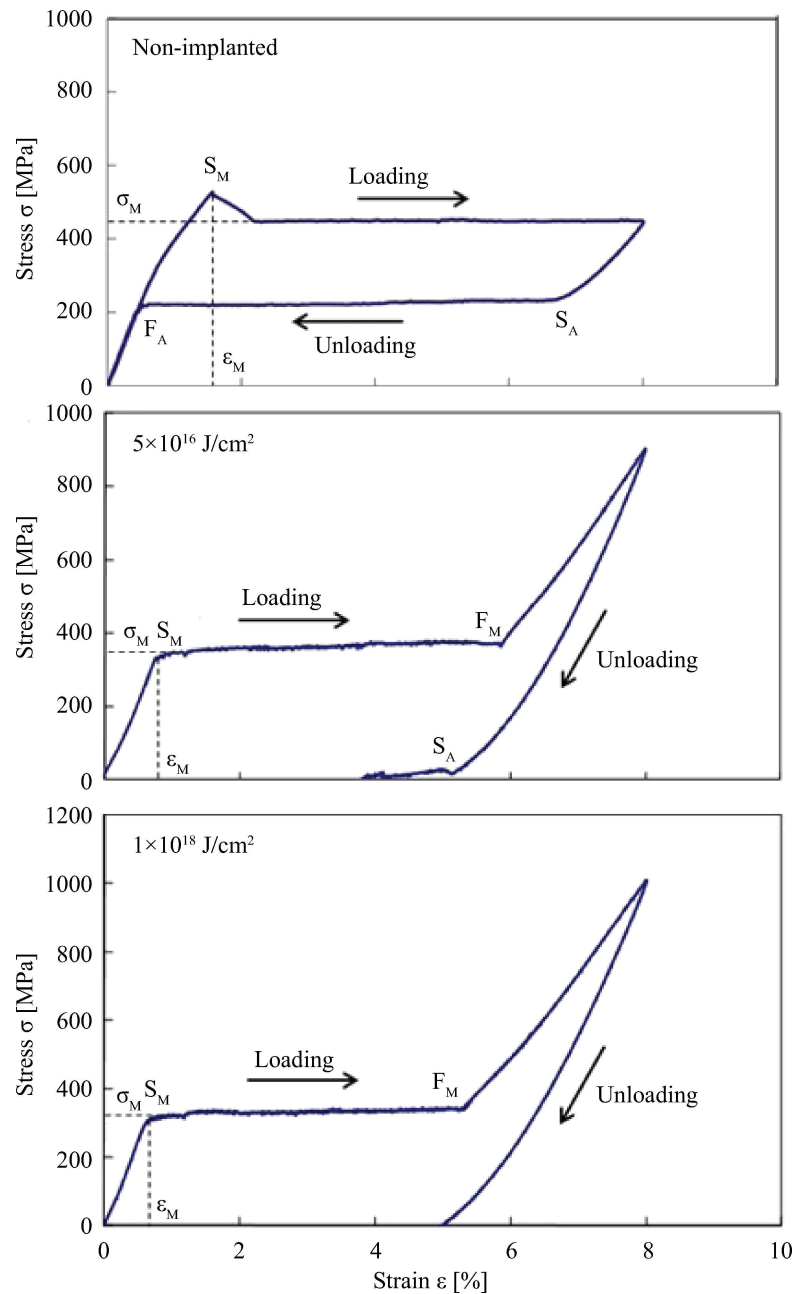
Fig. 3. Stress-strain curves of ion-implanted and non-implanted SMA wires.

the stress-induced martensitic transformation (SIMT) start and finish points, and reverse transformation start and finish points, respectively. The strain ε_M

represents the SIMT starting strain. If the dose of ion implantation increases, the upper yield stress σ_M decreases due to the SIMT. Although the ion-implanted region is limited in the surface layer, temperature of the wire increases during the ion implantation process. If the shape memory processing temperature is high, the upper yield stress σ_M decreases. Therefore, the same as in the shape memory processing, σ_M decreases due to the temperature rise during the ion implantation process. The stress-strain curve of a non-implanted wire draws a hysteresis loop during loading and unloading, showing the superelasticity (SE). The MT band propagates in the upper stress plateau. If the upper yield stress σ_M is high in the region of superelasticity, it is necessary for the stress to increase higher than the stress σ_M for the MT band propagation, resulting in the overshot at point S_M. In the case of ion-implanted wire with 5×10^{16} J/cm^2 the reverse transformation does not complete during unloading and the curve shows the partial SE. In the case of ion-implanted wire with 1×10^{18} J/cm^2 the reverse transformation does not appear during unloading and the residual strain of 5% appears after unloading. The residual strain disappears by heating under no-load, showing the shape memory effect (SME). As observed in Fig. 2, if a higher dose of implantation is applied, the reverse transformation temperatures increase. Therefore, both the upper and lower yield stresses decrease and the SME appears in place of the SE.

5. Bending fatigue property

5.1. Fatigue life

The relationships between the bending strain amplitude ε_a and the number of cycles to failure N_f for three kinds of wires obtained by the alternating-plane bending fatigue test at room temperature are shown in Fig. 4. The bending strain amplitude was obtained from the bending strain on the surface of the specimen at the fracture point. The specimen was fractured at the midpoint of two grips. As can be seen in Fig. 4, the larger the bending strain amplitude, the shorter the fatigue life is. If the bending strain amplitude is 4%, the fatigue lives of all materials are almost the same. If the bending strain amplitude is small, the fatigue life becomes longer in the case of higher dose of ion implantation.

The relationships between the bending strain amplitude and the number of cycles to failure shown on the logarithmic graph are almost expressed by straight lines for all materials. Therefore, the relationships can be expressed by a power function as follows:

$$(5.1) \qquad \varepsilon_a \cdot N_f^{\beta} = \alpha,$$

where α and β represent ε_a in $N_f = 1$ and the slope of the $\log \varepsilon_a - \log N_f$
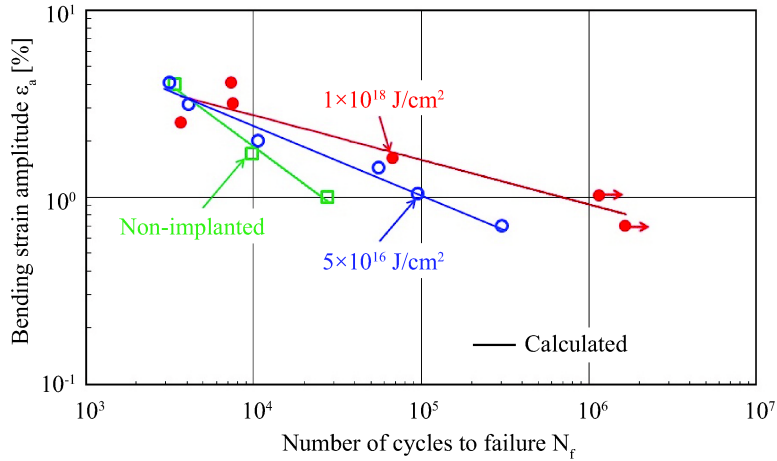
FIG. 4. Relationship between bending strain amplitude and the number of cycles to failure obtained by alternating-plane bending fatigue test.

curve, respectively. Each curves passes through a certain point at $\varepsilon_0 = 4\%$ and $N_0 = 4 \times 10^3$. Therefore, the relationships can be expressed by the following equation:

$$(5.2) \qquad \left(\frac{\varepsilon_a}{\varepsilon_0}\right) \cdot \left(\frac{N_f}{N_0}\right)^{\beta} = 1.$$

The calculated results of Eq. (5.2) are shown by solid lines in Fig. 4. The overall inclinations are well-approximated by the solid lines.

5.2. Fracture surface

In the case of an ion non-implanted wire, the fatigue crack initiates at the point of the maximum bending strain. If the nitrogen ion is implanted into the SMA wire, the fatigue crack initiates at the place different from the maximum bending strain point, depending on the dose of ion implantation and the bending strain amplitude. Let us discuss the influence of ion implantation on the fatigue crack initiation and growth by observing the fracture surface.

Figure 5 shows the microscope photographs of a fracture surface of a wire obtained by the fatigue tests for $\varepsilon_a = 1.04\%$ and 2% with 5×10^{16} J/cm^2. In Fig. 5, C_i denotes the center of ion implantation which corresponds to the point of the maximum bending strain; F_c denotes the point of the fatigue crack initiation. The crack nucleates at a certain point F_c on the surface of the wire and propagates towards the center in a sinuous radial pattern. Although small cracks are observed in both maximum bending strain sides of the wire, one single
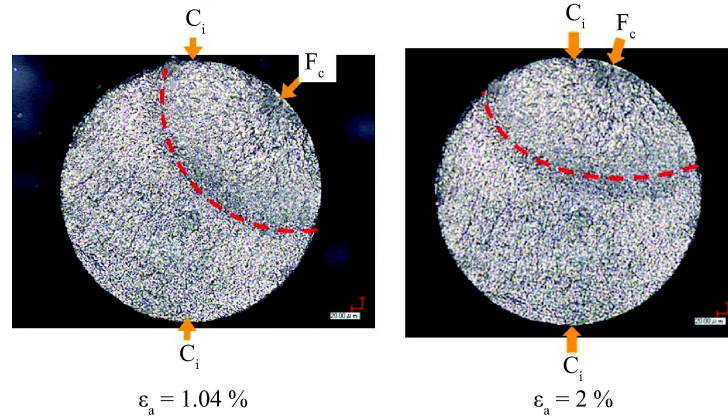
FIG. 5. Photographs of a fracture surface of the wire ion-implanted with 5×10^{16} J/cm^2 obtained by the fatigue test for $\varepsilon_a = 1.04\%$ and 2%. C_i is maximum bending strain point at the center of ion implantation, F_c is crack initiation point.

crack grows preferentially. Following the appearance of fatigue crack with a fan-shaped surface, unstable fracture finally occurs. For non-implanted wires, the point F_c coincides with the point C_i and the fatigue life is short.
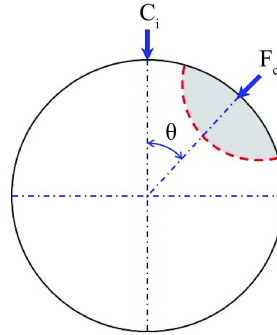

FIG. 6. Angle θ at crack initiation point F_c from the maximum bending strain point C_i at the center of ion implantation.

In order to clarify the fatigue crack initiation point F_c, the angle θ at the crack initiation point F_c from the maximum bending strain point C_i at the center of ion implantation is schematically shown in Fig. 6. The relationship between the crack initiation angle $|\theta|$ and the bending strain amplitude ε_a is shown in Fig. 7 for the non-implanted and ion-implanted wires. The larger the stain amplitude ε_a, the smaller the angle $|\theta|$ for ion-implanted wires is. The relationship between $|\theta|$ and ε_a is expressed by straight lines on the semi-logarithmic scale. Therefore, the relationship can be expressed as follows:

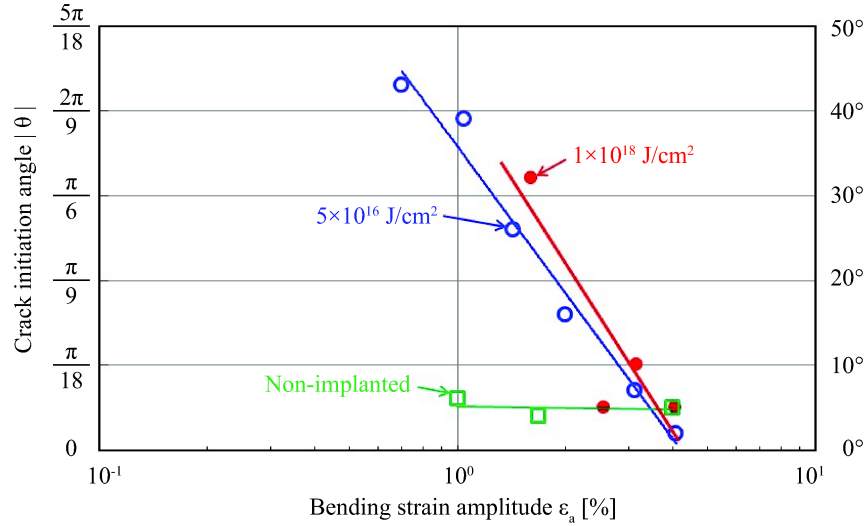(5.3) $$|\theta| = a \log \varepsilon_a + b.$$

FIG. 7. Relationship between angle at crack initiation point $|\theta|$ from maximum bending strain point at the center of ion implantation and bending strain amplitude ε_a.

The relationship can be rearranged as follows:

$$(5.4) \qquad \varepsilon_a = Ae^{B|\theta|}.$$

The values of coefficients are $A = 0.042$ and $B = -2.3$ for a wire with 5×10^{16} J/cm^2, and $A = 0.043$ and $B = -2.03$ for a wire with 1×10^{18} J/cm^2.

In the case of a non-implanted wire, $|\theta|$ is close to zero [14]. In the case of large ε_a for ion-implanted wire, $|\theta|$ is also close to zero. If ε_a is small, $|\theta|$ is large for ion-implanted wires, and the higher the dose of ion implantation, the larger the angle $|\theta|$ is, resulting in longer fatigue life. This means that the influence of ion implantation on the long fatigue life is effective in the case of small strain amplitude. Therefore, if ion is implanted on the whole surface of a wire and the wire is used in the region of small strain amplitude, a longer fatigue life must be achieved.

6. Influence of ion implantation on A_f, σ_M and β

Let us discuss the influence of ion implantation on the phase transformation temperature, tensile deformation property and fatigue life. As observed in the previous sections, if high dose of nitrogen ion is applied, the reverse transformation finish temperature A_f increases (Fig. 2), the upper yield stress σ_M decreases (Fig. 3) and the slope of the fatigue life curve β decreases (Fig. 4). The behavior of A_f and σ_M due to ion implantation is similar to that due to heat treatment

for shape-memorizing. If the heat treatment temperature is high, A_f increases and σ_M decreases. The ratio of change in σ_M and A_f, $\Delta\sigma_M/\Delta A_f$, between wires with non-implantation and $I_n = 1 \times 10^{18}$ J/cm^2 is 5.5 MPa/K. This value is close to the slope of the transformation line of TiNi SMA [15].

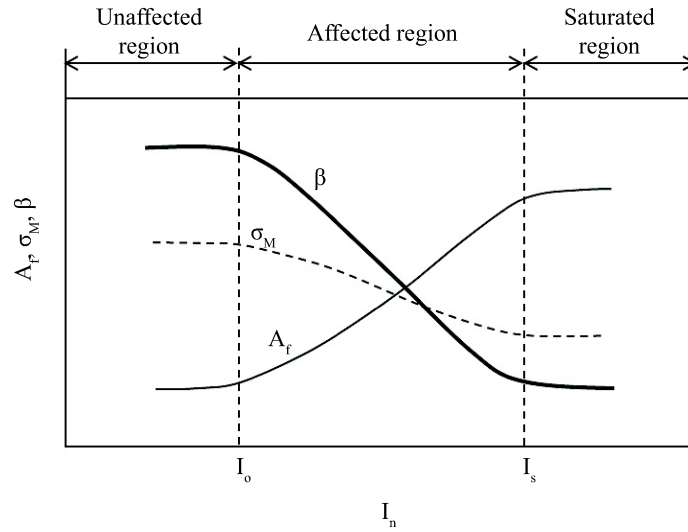FIG. 8. Schematic dependence of A_f, σ_M and β on I_n.

If the dose of ion implantation is small, the influence of ion implantation on A_f, σ_M and β is slight. If the dose of ion implantation is very high, these parameters may saturate a certain values. Considering these properties, the dependence of A_f, σ_M and β on the dose of ion implantation I_n may be schematically shown in Fig. 8. In Fig. 8, I_0 denotes a critical value of the dose of ion implantation at which the influence of I_n on the parameters starts to appear and these parameters change slightly below I_0. I_s denotes a value at which the influence saturates and these parameters change slightly above I_s. These parameters may change in the affected region between I_0 and I_s.

The dependence of A_f, σ_M and β on I_n obtained by the experiments is shown in Fig. 9. In Fig. 9, it is assumed that I_0 may exist around 2×10^{13} J/cm^2 and these parameters change linearly in the affected region as follows:

$$A_f = a_A \log_{10}(I_n/I_0) + b_A,$$

(6.1)
$$\sigma_M = a_\sigma \log_{10}(I_n/I_0) + b_\sigma,$$

$$\beta = a_\beta \log_{10}(I_n/I_o) + b_\beta.$$

The values of coefficients are $a_A = 5.43$ K, $b_A = 291$ K, $a_\sigma = -31.4$ MPa, $b_\sigma = 444$ MPa, $a_\beta = -0.0921$ and $b_\beta = 0.673$. The values of I_0 and I_s are
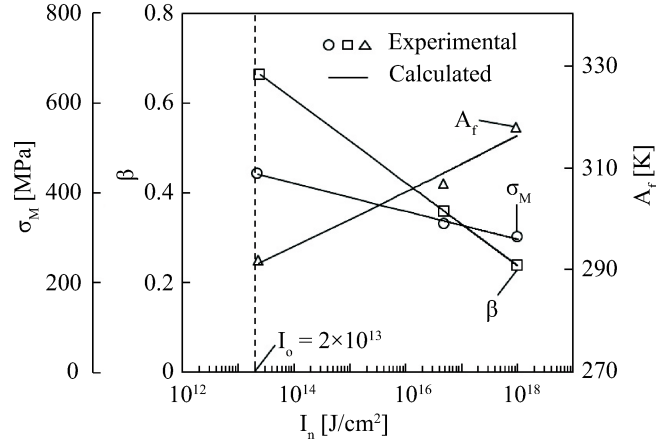
FIG. 9. Dependence of A_f, σ_M and β on I_n.

estimated as 2×10^{13} J/cm^2 and 1×10^{18} J/cm^2, respectively. The detail of I_0 and I_s is the future subject.

7. Conclusions

The nitrogen ion was implanted into TiNi SMA wires from two opposite directions, and the influence of implantation treatment on the phase transformation temperature, tensile deformation and bending fatigue properties was investigated. The results obtained are summarized as follows.

1. If the dose of ion implantation increases, the reverse transformation temperature increases.
2. Both the upper and lower yield stresses decrease in proportion to the dose of ion implantation. If the dose of ion implantation is high, the shape memory effect appears in place of the superelasticity in the non-implanted wire.
3. The larger the bending strain amplitude, the shorter the fatigue life is. If the strain amplitude is 4 %, the fatigue lives of all wires with and without ion implantation are almost the same. If the bending strain amplitude is small, the fatigue life becomes longer in the case of higher dose of ion implantation.
4. The fatigue crack nucleates at a certain point on the surface of the wire and propagates towards the center in a sinuous radius pattern. In the case of higher ion implantation in the region of small strain amplitude, the fatigue crack initiation point differs from the maximum bending strain point, resulting in longer fatigue life.

Acknowledgment

References

1. M. Wagner, T. Sawaguchi, G. Kausträter, D. Höffken, G. Eggeler, *Structural fatigue of pseudoelastic NiTi shape memory wires*, Materials Science and Engineering A, **378**, 105–109, 2004.

2. D.J. Wever, A.G. Veldhuizen, M.M. Sanders, J.M. Schakenrad, J.R. van Horn, *Cytotoxic, allergic and genotoxic activity of a nickel-titanium alloy*, Biomaterials, **18**, 1115–1120, 1997.

3. J. van Humbeeck, *Non-medical applications of shape memory alloys*, Material Science and Engineering A, **273-275**, 134–148, 1999.

4. J.K. Hirvonen, *Ion Implantation*, Academic Press, United States, 1980.

5. T. Asaoka, M. Mitsuo, *Effect of aluminium ion implantation on shape memory properties of titanium-nickel alloy*, Materials Transaction, JIM, **41**, 6, 739–744, 2000.

6. H. Pelletier, D. Muller, P. Mille, J. Grob, *Structural and mechanical characterization of boron and nitrogen implanted NiTi shape memory alloy*, Surface and Coating Technology, **158-159**, 309–317, 2002.

7. A.D. Pogrebnjak, E.A. Bazyl, *Modification of wear and fatigue characteristics of Ti–V–Al alloy by Cu and Ni ion implantation and high-current electron beam treatment*, Vacuum, **64**, 1, 1–7, 2001.

8. O.M. Ivasishin, A.D. Pogrebnjak, S.N. Bratushka, *Nanostructured layers and coating formed by ion-plasma fluxes in titanium alloys and steels*, Kyiv, Akademperiodyka, 284, 2011.

9. N. Levintant-Zayonts, S. Kucharski, *Surface characterization and wear behavior of ion implanted NiTi shape memory alloy*, Vacuum, **83**, S220–S223, 2009.

10. T. Czeppe, N. Levintant-Zayonts, Z. Swiatek, M. Michalec, O. Bonchyk, G. Savitskij, *Inhomogeneous structure of near-surface layers in the ion-implanted NiTi alloy*, Vacuum, **83**, S214–S219, 2009.

11. G. Giulio, P. Oscar Faciola, B. Fernando Branco, M.A.Z. Vasconcellos, C. Celso Luiz, *Cyclic fatigue resistance of rotary nickel-titanium instruments submitted to nitrogen ion implantation*, Journal of Endodontics, **36**, 7, 1183–1186, 2010.

12. C. Federico Brilhante Wolle, M. Antonio Zen Vasconcello, R. Hinrikhs, A. Niederauer Becker, F. Branco Arletta, *The effect of argon and nitrogen ion implantation on nickel-titanium rotary instruments*, Journal of Endodontics, **35**, 7, 1558–1562, 2009.

13. Y. Furuichi, H. Tobushi, T. Ikawa, R. Matsui, *Fatigue properties of a TiNi shape-memory alloy wire subjected to bending with various strain ratios*, Proc. Instn. Mech. Engrs., **217**, Part L: J. Materials: Design and Appl., 93–99, 2003.

14. R. Matsui, H. Tobushi, Y. Furuichi, H. Horikawa, *Tensile deformation and rotating-bending fatigue properties of a highelastic thin wire, a superelastic thin wire, and a superelastic thin tube of NiTi alloys*, Trans. ASME, J. Eng. Mater. Tech., **126**, 384–391, 2004.

15. K. Tanaka, F. Nishimura, H. Tobushi, *Transformation start lines in TiNi and Fe-based shape memory alloys after incomplete transformations induced by mechanical and/or thermal loads*, Mech. Mater., **19**, 271–280, 1995.

—————